# Nanoscale

Accepted Manuscript


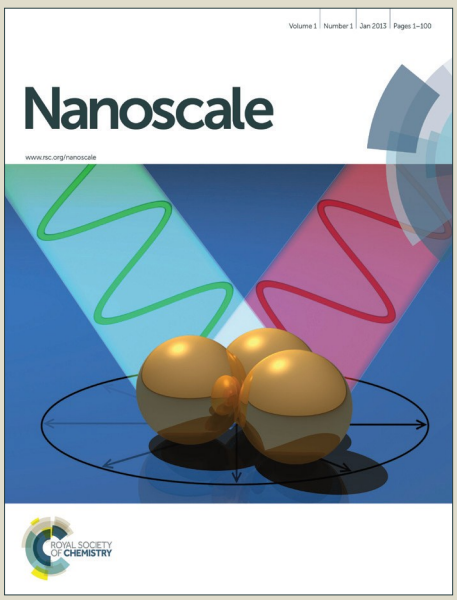





ROYAL SOCIETY OF CHEMISTRY

www.rsc.org/nanoscale

Journal Name

ARTICLE

# Novel porous calcium aluminate/phosphate nanocomposites: in situ synthesis, microstructure and permeability

Received 00th January 20xx,
Accepted 00th January 20xx

DOI: 10.1039/x0xx00000x

www.rsc.org/

Jingzhou Yang,[a,b,c,*], Xiaozhi Hu,[a,*] Juntong Huang[d], Kai Chen[e], Zhaohui Huang[f], Yangai Liu[f], Minghao Fang[f], and Xudong Sun[g]

Permeable porous nanomaterials have extensive applications in engineering fields. Here, we report a novel system of porous calcium aluminate/phosphate (CaAl-CaP) nanocomposites fabricated by a pore generator free processing. The CaAl rich samples have close micropores and are not permeable. Interestingly, the CaP rich composites have a unique three-dimensional nanosieve structure with interconnected nanopores and exhibit excellent liquid permeability and adsorbability. The pore size has a narrow distribution of 200 - 500 nm. The CaAl nanoplatelets in CaP rich composite have a thickness of 202 nm, a diameter of 1600 nm and an aspect ration of 8. The porosity is from 19 % to 40 %. The bending strength and compressive strength are 40.3 MPa and 195 MPa, respectively. The CaP rich nanocomposite is highly permeable so that a water droplet can completely penetrate in 10 seconds (1 mm thick disk). The blue dye can be desorbed in 45 min by ultrasonic vibration. Given the nanosieve porous structure, good permeability/adsorbability and high mechanical properties, the CaP rich nanocomposite has a big potential in applications for chemical engineering, biomedical engineering and energy/environmental engineering.

## 1 Introduction

Nano/microporous permeable ceramics with high mechanical properties are promising for many engineering applications including hard tissue engineering scaffolds, controlled drug release carriers, fluid/gas-flow filters, catalyst supports, bioreactors, thermal sinks/convertors, sound/thermo-insulation building materials, electrodes for new power-generation systems.[1-10] Much effort has been made to fabricate porous ceramic products with various microstructures for special emerging applications, leading to fast development of relevant manufacturing techniques. For instance, polymer templates burn-out,[11-15] freeze casting/drying,[16,17] liquid/gel foaming,[18,19] selective dissolution[20,21] have been shown to be able to make a great variety of bulk porous ceramics. **However the current techniques require addition of organic or inorganic pore generators and the resultant nano/micro porous ceramics have relatively low strength and wide pore size distribution. Nano/microporous calcium phosphate ceramics were fabricated by sacrificing polymer templates. The bending strength and compression strength were 15-20 MPa and 70-110 MPa[22,23], respectively. Silicon carbide and silicon oxide based nanoporous ceramics were developed by polymer precursor burn-out method[24,25]. Wide pore size distribution was found in these porous ceramics. Alternative manufacturing methods are needed to fabricate uniform three dimensional (3D) nanoporous structures with high strength and permeability.**

We use solid-state reaction and in situ pore forming method to fabricate novel porous calcium aluminate/phosphate (CaAl-CaP) nanocomposites. The manufacturing process does not involve any pore generators. The resultant composite is expected to have uniform nanoporous structure, **high mechanical properties, narrow pore size distribution and** excellent liquid permeability. This paper covers in situ synthesis, microstructure characterization, phase composition determination, porosity/pore size analysis, and permeability investigation.

[a] School of Mechanical and Chemical Engineering, University of Western Australia, Perth, WA 6009, Australia
E-mail: xiao.zhi.hu@ uwa.edu.au.
[b] Department of Medicine, Brigham and Women's Hospital, Harvard Medical School, Boston, MA 02115, USA
E-mail: jyang@bwh.harvard.edu.
[c] Harvard-MIT Division of Health Science and Technology, Massachusetts Institute of Technology, Cambridge, MA 02139, USA
[d] College of Engineering, Mathematics and Physical Sciences, University of Exeter, Exeter EX44QF, UK
[e] National Engineering Research Centre for Rare Earth Materials, General Research Institute for Nonferrous Metals, Grirem Advanced Materials Co., Ltd., Beijing 100088, P.P. China
[f] School of Materials Science and Technology, China University of Geosciences (Beijing), Beijing 100083, P. R. China
[g] Key Laboratory for Anisotropy and Texture of Materials (Ministry of Education), Northeastern University, Shenyang, 110004, P. R. China

## 2 Experimental

### 2.1 Materials and processing

Alumina ($\alpha$-$Al_2O_3$) (AKP50, purity > 99.99 %, < 300 nm, Sumitomo, Japan) and Hydroxyapatite (HA) (< 200 nm, Sigma-Aldrich Co., USA) powders were selected as starting materials for the proposed CaAl-CaP nanocomposites. Polyvinyl alcohol PVA (9 wt% in concentration) solution was used as temporary binder. Four formulas of composites (**CP10,** CP30, CP50 and CP90) were made with HA addition of 10 wt%, 30 wt%, 50 wt% and 90 wt%. The alumina and HA powder mixtures were prepared through wet ball milling in distilled water for 24 h. The slurries were fully dried at 60 °C for 48 h and then the powder blocks were crushed/ground to

fine powders below 10 µm. Small green disks and strips were fabricated by die pressing under a pressure of 60 MPa using a circle die (12 mm in diameter) and a strip die (4 mm×6 mm). The compacts were sintered at 1300 °C for 2 h in a muffle furnace (KSL-1700X-A4, MTI Corporation, USA). The heating rate was 300 °C/h. Fully dense pure HA ceramic disks were also produced as control materials for permeability test. To investigate the effects of pre-sintered HA microparticles on the porosity and pore size of CaP rich nanocomposite (CP90), four formulas of samples (CP90-1, CP90-2, CP90-3 and CP90-4) were prepared with HA microparticle addition of 0 wt%, 20 wt%, 40 wt% and 80 wt%. Pure HA powders were pressed to compacts using a square steel die (40 mm×40 mm) under a pressure of 40 MPa, followed by pre-sintering at 900 °C for 2 h. The pre-sintered HA blocks were crushed to microparticles with a diameter of 50-100 µm determined by standard sieves. 10 wt% alumina powder containing HA based mixtures with different HA powder-particle mass ratios were prepared through wet ball milling. HA microparticle containing compacts were manufactured with same drying, die pressing and sintering protocols of powder only compacts.

### 2.2 Characterizations of microstructure and grain morphology

Field Emission Scanning Electron Microscope (FESEM) Zeiss 1555 (Oberkochen, Germany) was used to observe the microstructure and grain morphology of CaAl-CaP nanocomposites. **SEM image based ceramography method was employed to analyse grain size. ImageJ software was used to do line-fraction. One hundred grains were randomly selected and the statistical grain size was calculated from the number of grains intersecting a line of known length.** Energy Dispersive Spectroscopy was employed to detect elements in the ceramic grains. To visualize cross-section microstructure, the samples were embedded in epoxy resin (EpoFix epoxy, Struers A/S, DK-2750 Ballerup, Pederstrupvej 84, Denmark) and polished with diamond suspension with a final size of 1 µm. The resin embedding was essential to preserve the porous structure during sectioning and polishing.

### 2.3 Determination of phase composition, porosity and mechanical properties

Phase compositions of **CaAl rich nanocomposites (CP10, CP30, CP50) and CaP rich nanocomposites (CP 90)** were characterized with X-ray diffraction (Panalytical Empyrean diffractometer, PANalytical B.V., EA ALMELO, Netherlands) using CuKa1 radiation at a scanning rate of 1.2 °/min. The porosity was measured by Archimedes' principle and mercury intrusion method. **Archimedes' principle is the most common method for porosity measurement. The equation for porosity calculation is P=[(M3-M1)/(M3-M2)] X 100%. P - porosity; M1 - dry mass value measured in the air; M2 - wet mass value measured in the liquid; M3 - wet mass value (after fully absorbing immersion liquid) measured in the air. Statistical porosity value was generated based on six samples. We did vacuum immersion in lubricant oil for 30 mins to prepare samples for measuring M2 and M3.**

**The pore size (by volume) distribution was determined by mercury porosimetry. Pressure is applied to force mercury into smaller and smaller pores. Measuring the applied pressure and the intrusion volume, the pore size distribution can be calculated. The factors we used are as follows. Evacuation pressure: 50 µmHg; Evacuation time: 5 mins; Mercury filling pressure: 0.43 psia; Equilibration time: 10 secs; Pressure range: 0.10 to 60000.00 psia; Total intrusion volume: 0.0936 mL/g.**

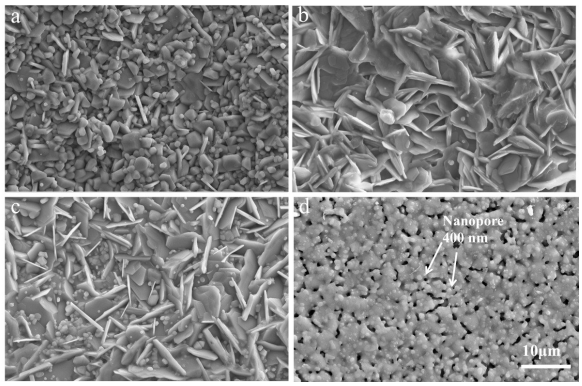


**Fig. 1.** As-sintered surface microstructure of CaAl-CaP nanocomposites. (a) CP10; (b) CP30; (c) CP50; (d) CP90.

**Table 1** Thickness, diameter and aspect ratio of CaAl nanoplatelets in CaAl-CaP nanocomposites

| Materials | CP10 | CP30 | CP50 | CP90 |
|---|---|---|---|---|
| Thickness (nm) | 263 ± 27.4 | 450 ± 37 | 211 ± 20.8 | 202 ± 34.8 |
| Diameter (µm) | 6.7 ± 0.37 | 7.5 ± 0.4 | 5.8 ± 0.3 | 1.6 ± 0.18 |
| Aspect ratio | 25.5 | 16.7 | 27.6 | 8 |

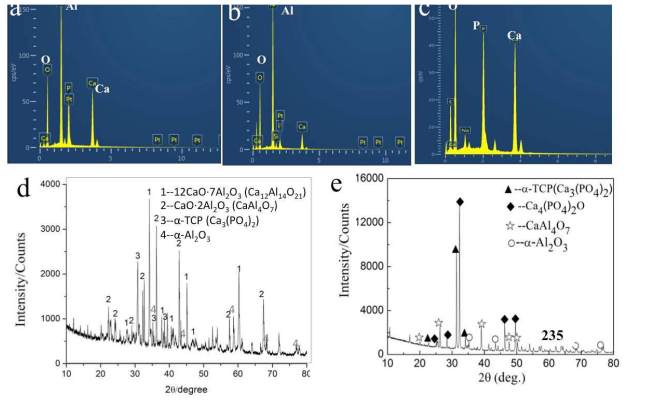


**Fig. 2.** EDS and XRD spectrums confirming the chemical composition and phase composition of CaAl-CaP nanocomposites. (a) elements in the nanoplatelet (+1 in Fig. 1d); (b) elements in the nanoparticle (+2 in Fig. 1d); (c) elements in the microparticle (+3 in Fig. 1d); (d) XRD result showing phase composition of CaAl rich nanocomposite; (e) XRD result showing phase composition of CaP rich nanocomposite.

Three point bending test and compression test were carried out using Instron 4301 (Max 5 kN)/5982 (Max 100kN) (Instron Company, Norwood, MA 02062-2643, USA) to study the mechanical properties. For bending test, the sample dimension was 3 × 4 × 40 mm, crosshead speed was 0.5 mm/min and the jig span was 24 mm. For compression test, the sample dimension was 11.2 × 11.2 mm (Φ × h). The load speed was 0.1 mm/min.

### 2.4 Characterization of permeability and adsorption/desorption ability

The permeability, adsorbability and desorbability of the nanocomposites were investigated by water penetrating test. Water was colorized with blue dye. Then the blue water was dropped on the surface of fully sintered nanocomposite and HA ceramic disk. The processing of water permeation and adsorption were recorded by high-speed photography with an interval of 0.2 second. The area changes of water droplet and blue stain were measured. **Desorption of blue dye was tested by ultrasonic vibration for 45 min. The power rate was 120 W, frequency rate was 80 KHz and working temperature was 25 °C.**

## 3 Results and discussion

It has been reported that addition of alumina in hydroxyapatite can induce transformation of hydroxyapatite (HA) to tricalcium phosphate (TCP) with release of gassy water at high temperature. The reaction is illustrated in equation (1).[26,27] We use this fundamental to fabricate porous calcium aluminate/phosphate (CaAl-CaP) nanocomposites without any extra pore generators. Four batches of samples (10CP10, CP30, CP50 and CP90) with increasing addition of HA in the raw powder mixture were manufactured by solid-state reaction and in situ pore forming at 1300 °C.

$$Ca_{10}(PO_4)_6(OH)_2 + Al_2O_3 = Ca_x(PO_4)_y + CaO{\cdot}nAl_2O_3 + H_2O(g) \quad (1)$$

**Fig. 1 presents as-sintered surface overviews of the CaAl-CaP composites. The matrix of CaAl rich samples (CP30 and CP50) is composed of CaAl nanoplatletes with CaP micrograins scattered (Fig. 1(a,b)). Although the CaAl rich sample has a relatively dense structure, there are still some micropores due to the gassy water releasing and nanoplatlete interlacing. CP10 only has limited CaAl nanoplatletes because alumina is excessive in the raw powder mixture. Nanosieve structure is found in CaP rich sample (Fig. 1 (d)).** Table 1 displays that the nanoplatletes in CP30 have a thickness of 450 ± 37 nm, a diameter of 7.5 ± 0.4 μm and an aspect ration of 16.7. Those are 211 ± 20.8 nm, 5.8 ± 0.3 μm and 27.6 for CP50. CaP rich sample of CP90 have much smaller CaAl nanoplatletes with the thickness, diameter and aspect ration of 202 ± 34.8 nm, 1.6 ± 0.18 μm and 8, respectively. Nanopores with a diameter of around 200 nm are found in CaP rich sample. Fig 2 shows the EDS results of ceramic grains with different morphologies in the composite and XRD spectrums of CaAl rich sample (CP30) and CaP rich sample (CP90). The main phases include TCP, monocalcium dialuminate ($CaO{\cdot}2Al_2O_3$), and dodecacalcium hepta-aluminate ($12CaO{\cdot}7Al_2O_3$) in CaAl rich sample. TCP, tetracalcium phosphate (TTCP), monocalcium dialuminate are found in CaP rich sample. Both samples have a minor phase of alpha alumina. In Fig. 1(d), The nanoplatlete (+1) is calcium aluminate, the equiaxed micrograin (+3) is calcium phosphate and the equiaxed nanograin (+2) is alumina. To confirm if the CaAl rich sample has a porous structure, fracture surface was observed under SEM. Typical images are shown in Fig. 3. Micropores are found in the inner body.

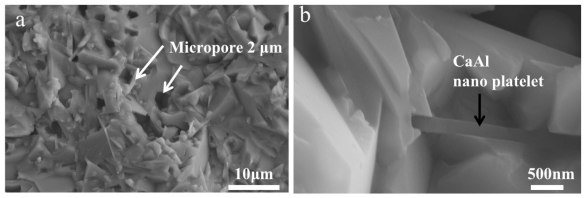


**Fig. 3.** Fracture surface microstructure of CaAl rich nanocomposites. (a) Overview and close-up of showing the close nanopores and nanoplatelets.

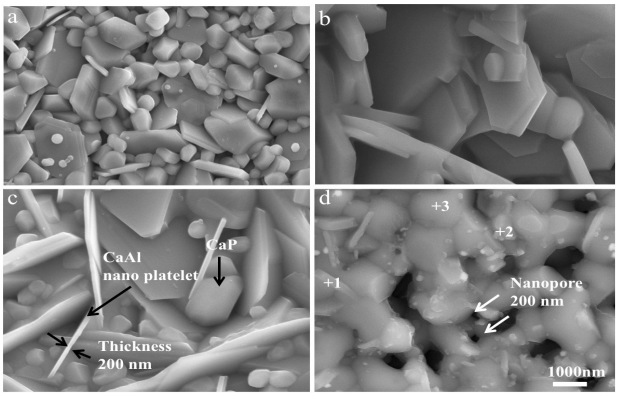


**Fig. 4.** Grain morphologies and porous structure of CaAl-CaP nanocomposites with different formulas of starting powder mixtures. (a) CP10; (b) CP30; (c) CP50; (d) CP90. CaAl nanoplatelets have a thickness of around 200 nm. Nanopores are found in CaP rich sample.

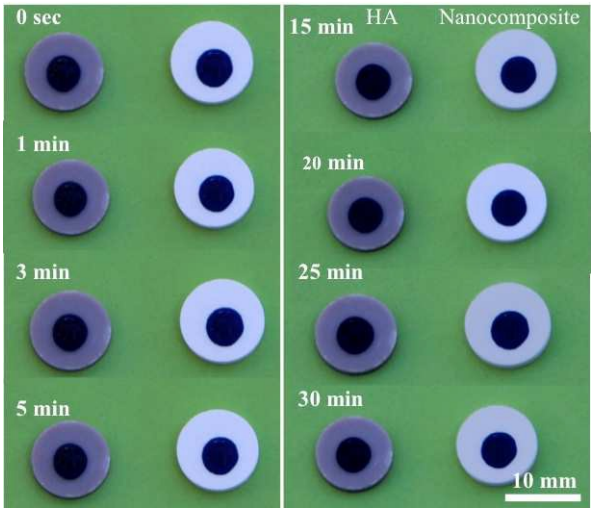


**Fig. 5.** Digital photos showing CaAl rich nanocomposite is not permeable and does not adsorb liquid. Left sample is HA (thickness=1 mm; diameter=8 mm). Right sample is nanocomposite (thickness=1 mm; diameter=10 mm).

**Fig. 4 shows the detailed microstructure features and grain morphologies of CaAl-CaP nanocomposites. As can be seen, CP30 and CP50 have more and bigger CaAl nanoplatletes that are interlocked with each other.** Alumina and HA ratio in the raw powder mixture has notable effects on the microstructure and porosity of CaAl-CaP composites. CaAl rich sample has a micro close-pore structure, while CaP rich sample has a nano open-pore structure. And CaP rich sample has smaller nanoplatletes than CaAl rich sample.

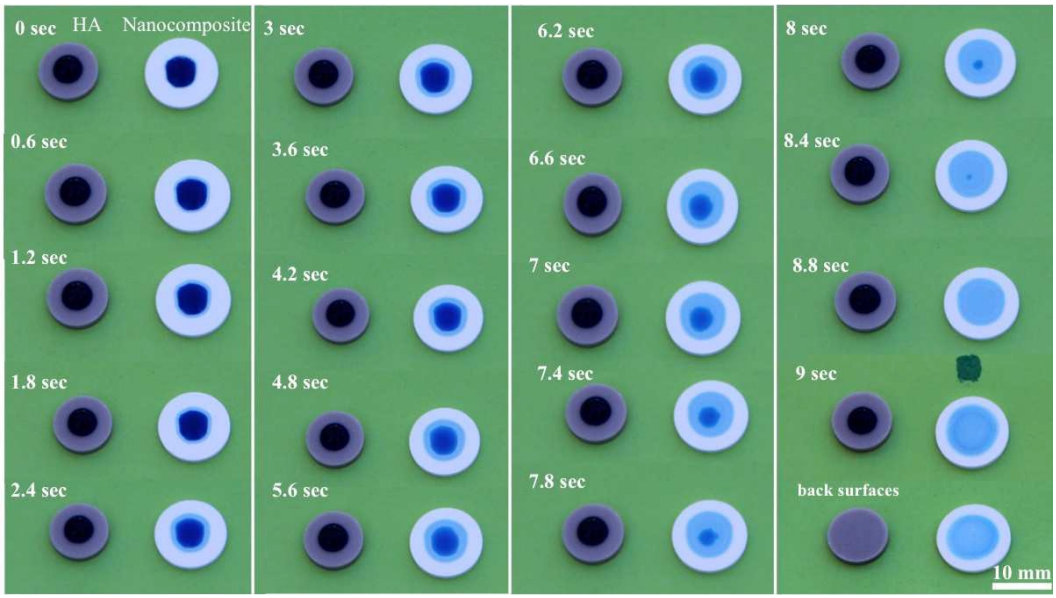


**Fig. 6.** Digital photos showing CaP rich nanocomposite has excellent permeability and adsorption ability. A water droplet (colorized by blue dye) penetrated the nanoporous ceramic disk with adsorption of blue dye in 9 seconds. Left sample is HA (thickness=1 mm; diameter=8 mm). Right sample is nanocomposite (thickness=1 mm; diameter=11 mm).

In chemical engineering, biomedical engineering and environmental engineering applications, nano/microporous materials normally require a high permeability and adsorbability. For instance, liquid/gas separation needs permeable porous materials as filters. Bone/osteochondral tissue regeneration and localized drug/growth factor release demand biomaterials with permeable porous structure as scaffolds and carriers. Water purification and treatment of oil pollution seek porous materials with high permeability and adsorbability. We used water penetrating method and ultrasonic vibration to evaluate the permeability and adsorption/desorption ability of the developed porous CaAl-CaP nanocomposites. Blue dye colorized water was dropped on the surfaces of fully sintered nanocomposite and HA ceramic disks. It can be seen from Fig. 5 that water droplet did not penetrate into CaAl rich disk and was not adsorbed at all during the testing time of 45 min. This confirmed that the CaAl rich nanocomposite is not permeable due to its close-pore structure. Interestingly, water droplet penetrated the CaP rich sample in 10 seconds (Fig. 6). The sample was colorized by the blue dye. From 0 to 6.2 second, the disk gradually adsorbed the blue water droplet. From 6.6 second, the adsorption became much faster. The droplet totally penetrated the disk at 9 second confirmed by blue stain on green paper. The results indicate that CaP rich nanocomposite has good permeability and adsorbability because of its 3D interconnected nanosieve structure. Fig. 7 shows changes of water droplet size and blue stain area on the disk with time going. The initial droplet size and blue stain area were both 19.6 $mm^2$. The droplet size did not change until 5 second, but the blue stain area increased to 28.6 $mm^2$ at 2 second and 38.5 $mm^2$ at 5 second. Then water droplet became smaller very fast. This indicates the water was adsorbed by the sample. The final area of blue stain was 44.2 $mm^2$. The permeability test results suggested that water can penetrate CaP porous nanocomposites and blue dye was adsorbed simultaneously. The blue dye can be desorbed by ultrasonic vibration (Fig. 8). After 6 min, around half of blue dye was desorbed. After 45 min, the blue dye was almost totally desorbed from the sample. The CaP rich nanocomposite exhibits high permeability and fast adsorption/desorption capability so that it can be potentially used in a number of engineering fields.

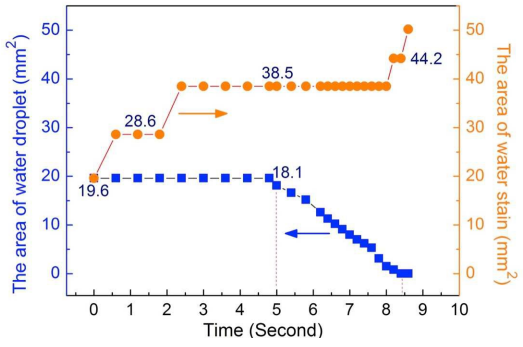


**Fig. 7.** Area change of water droplet and blue stain on the nanocomposite disk with time going.

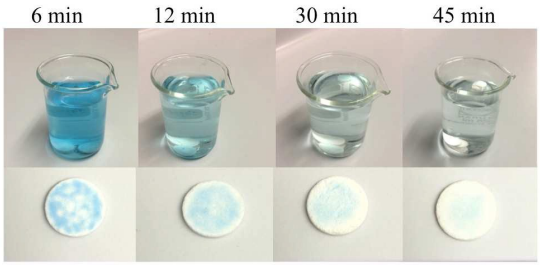


**Fig. 8.** Digital photos showing the blue dye desorption behaviour of CaP rich nanocomposite by ultrasonic vibration.

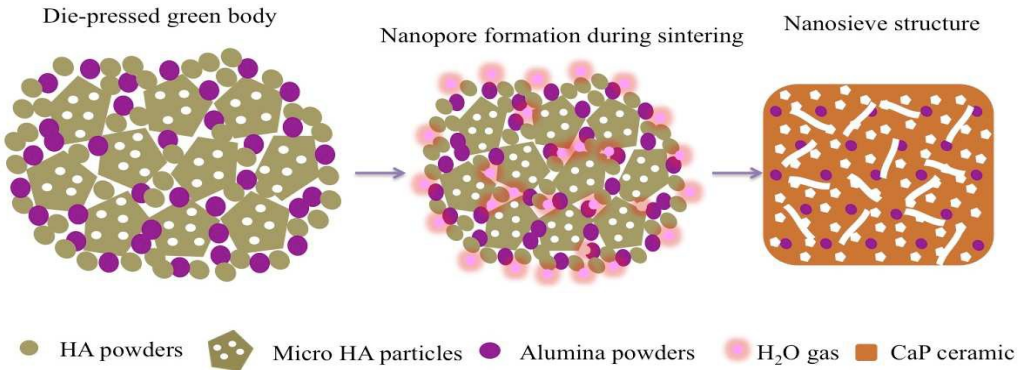


**Fig. 9.** Nanosieve structure forming mechanism of in situ gas releasing and porous micro particle wedding.

In bone tissue engineering, permeable porous bioceramics are used as scaffolding materials for bone and osteochondral tissue regeneration. Although macroporous bone scaffolds are osteoconductive to promote bone ingrowth,[28-30] their immediate load-bearing capacity is inadequate for reconstruction of large-scale and load-bearing bones. The typical compressive strength of macro-porous ceramic scaffold is normally around 5-32 MPa[6,30] and the typical bending strength is merely few MPa.[31,32] Therefore micro/nanoporous bioceramics have been studied for improved mechanical properties and good osteoconductivity. It has been reported that interconnected micro/nano-scale porosity and

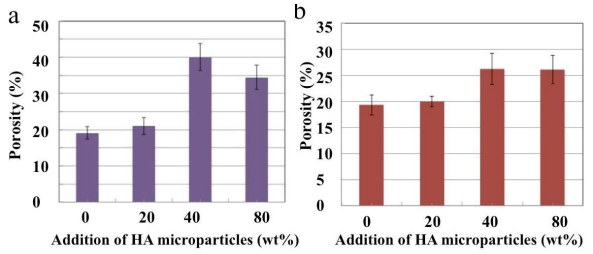


**Fig. 10.** Porosity of CaP rich nanosieve composites. (a) Result from archimedes' method; (b) Result from mercury intrusion method.

structure features have a notable positive effect on the osteoconductivity and bone ingrowth rate[29-31, 33-35] due to the enhancement of nutrient transportation. Furthermore, recent studies have proved that artificially synthesized microporous CaP ceramics showed excellent osteoinductivity that was comparable to autologous bone grafts.[1] Osteoinductivity and osteoconductivity are required for bioceramics to repair large-scale bone defects. It should be pointed out that the CaP rich porous nanocomposite exhibits high mechanical properties. The bending strength and compressive strength are 40.3 MPa and 195 MPa matching those of natural cortical bones (Table 2). Apparently the present CaP rich nanocomposite, with a permeable nanoporous structure and high strength, is promising as bone scaffolds for restoration of large-scale and load-bearing bones. Ceramic based drug delivery carriers have been developed for controlled slow drug release.[40-42] Nanoporous structure was proven to have better drug-delivery properties in terms of controlled release rate and efficiency.[3, 43-44] Micro/nano porous permeable ceramics have also been investigated as water purification sieves,[45-49] pollutant (e.g. oil, metal ions) capturers,[45-48] fluid/gas separation filters,[49, 50, 53] catalytic supporter/reactors[10, 54, 55] and thermal sinks/convertors,[56, 57] etc. It is believed that the present porous ceramic nanocomposite with narrow pore size distribution of 200 nm to 500 nm has potential applications in biomedical engineering, chemical engineering, environmental engineering and energy engineering.

The porosity of CaP rich nanocomposite (CP90-1) is 19.1 ± 1.7 % achieved by in situ gassy water releasing, a pore generator free method. For some application, higher porosity would be required. To increase the porosity, we modified the processing with addition of porous HA microparticles in the raw mixtures (Fig. 9). Micro

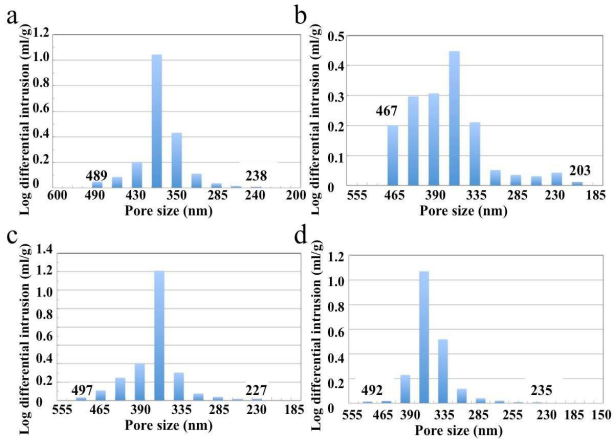


**Fig. 11.** Pore size distribution of CaP rich nanosieve composites. (a) CP90-1; (b) CP90-2; (c) CP90-3; (d) CP-90-4.

**Table 2** Strengths of porous CaP rich nanocomposite, CaP scaffolds, natural bone and dense CaP ceramic.

| Materials | Bending strength (MPa) | Compressive strength (MPa) |
|---|---|---|
| Present CaP porous nanocomposite | 40.3 ± 3.8 | 195 ± 15.5 |
| CaP ceramic scaffold | 2 - 3.5[31, 32] | 5 - 32[6, 33] |
| Compact/cortical bone | 50 - 300[36] | 170 - 193[37] |
| Pure dense CaP ceramic | 94 ± 26[38] | 419 ± 28[39] |

**Table 3** Median nanopore diameters by volume of CaP rich nanocomposites.

| Materials | CP90-1 | CP90-2 | CP90-3 | CP90-4 |
|---|---|---|---|---|
| median pore diameter (nm) | 401 | 383 | 363 | 404 |

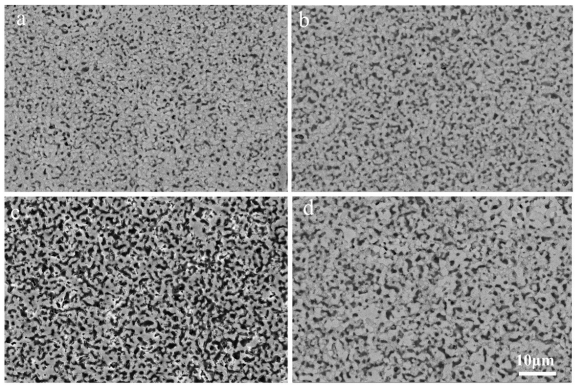


**Fig. 12.** Overview of polished cross-section showing interconnected porous structure of CaP rich nanosieve composites. (a) CP90-1; (b) CP90-2; (c) CP90-3; (d) CP-90-4.

ceramic particles have been used to make microstructural-engineered metal-ceramic network composite.[58, 59] We hope porous microparticle wedding in combination of in situ gas releasing can increase the porosity of CaP rich nanocomposite. Fig. 10 shows the porosity change with respect to addition of microparticles. As can be seen, the porosity increased to 40.1 ± 3.7 % (determined by Archimedes' principle) by adding 40 wt% microparticles (CP90-3).

The result from mercury intrusion method was 26.2 ± 3.0 %. There was an obvious increment of porosity confirmed by both methods. As shown in Table 3, the median pore size decreased from 400 nm (CP90-1) to 363 nm (CP90-3). The pore size distribution kept to the range of 200 nm to 500 nm (Fig. 11). Fig. 12 displays polished cross-section structure of samples CP90-1 to CP90-4. Nanopores are interconnected to form microchannels and 3-D porous network structure that contribute to the high permeability and adsorbability. Sample CP90-3 has the best nanosieve structure with the highest porosity. It was demonstrated that addition of porous microparticles, as a pore generator free strategy, can effectively increase the porosity of ceramic nanocomposites.

## 4 Conclusions

Porous calcium aluminate/phosphate nanocomposites were fabricated by high temperature solid-state reaction and in situ pore forming method from alumina and hydroxyapatite. The main phases are tricalcium phosphate, tetracalcium phosphate, monocalcium dialuminate, and dodecacalcium hepta-aluminate. Gassy water release during reaction resulted in the nanoporous structure. The calcium phosphate rich composite has an uniform nanosieve network architecture with narrow pore size distribution of 200 nm to 500 nm. Calcium aluminate nanoplatelets (thickness 200 nm and diameter 1600 nm) were located at the boundaries of or embedded in calcium phosphate micrograins. The bending strength and compressive strength are 40.3 MPa and 195 MPa, respectively. The calcium phosphate rich composite exhibited excellent liquid permeability and reversible dye adsorption ability. The porosity increased to 40 % from 19 % with increasing microparticles to 40 wt%. Given the nanosieve porous structure, good permeability/adsorbability and high mechanical properties, this nanocomposite can be potentially used for load-bearing bone defect repair, controlled drug delivery, fluid filtration, water purification, etc.

## Acknowledgements

This research was supported under Australian Research Council's Discovery Projects funding scheme (project number DP110105296) and Faculty of Engineering, Computing and Mathematics, University of Western Australia, Small Research Development Grant 2013-2014. J Yang would like to thank Australian Endeavour Fellowship. The authors acknowledge the facilities, and the scientific and technical assistance of the Australian Microscopy & Microanalysis Research Facility at the Centre for Microscopy, Characterisation & Analysis, University of Western Australia, a facility funded by the University, State and Commonwealth Governments.

## References

1 H. Yuan, H. Fernandes, P. Habibovic, J. de Boer, A. M. C. Barradas, A. de Ruiter, W. R. Walsh, C. A. van Blitterswijk and J. D. de Bruijn, *PNAS,* 2010*,* **107,** 13614.
2 H. O. Mayr, J. Klehm, S. Schwan, R. Hube, N. P. Südkamp, P. Niemeyer, G. Salzmann, R. von Eisenhardt-Rothe, A. Heilmann, M. Bohner and A. Bernstein, *Acta Biomater.,* 2013, **9,** 4845.
3 D. A. LaVan, T. McGuire and R. Langer, *Nature Biotech.*, 2003, **21,** 1184.
4 C.-L. He, G.-Y. Xiao, X.-B. Jin, C.-H. Sun and P. X. Ma, *Adv. Funct. Mater.,* 2010, **20,** 3568.
5 A. R. Boccaccini, F. Chicatun, J. Cho, O. Bretcanu, J. A. Roether, S. Novak and Q. Chen, *Adv. Funct. Mater.,* 2007, **17,** 2815.
6 H. R. R. Ramay and M. Zhang, *Biomaterials,* 2004, 25, 5171.
7 F.-Q. Sun, W.-P. Cai, Y. Li, L.-C. Jia and F. Lu, *Adv. Mater.,* 2005, **17,** 2872.
8 H. Verweij, *Adv. Mater.,* 1998, **10,** 1483.
9 D. Han, X.-J. Liu, F.-R. Zeng, J.-Q. Qian, T.-Z. Wu and Z.-L. Zhang, *Scientific Reports,* 2012, **2,** 462.
10 A. Julbe, D. Farrusseng and C. Guizard, *J. Membrane Sci.,* 2001, **181,** 3.
11 S. Kuiper, C. J. M. van Rijn, W. Nijdam and M. C. Elwenspoek, *J. Membrane Sci.,* 1998, **150,** 1.
12 S. K. Padmanabhann, F. Gervaso, M. Carrozzo, F. Scalera, A. Sannino and A. Licciulli, *Ceram. Int.,* DOI:10.1016/j.ceramint. 2012.06.073.
13 J. M. Taboas, R. D. Maddox, P. H. Krebsbach and S. J. Hollister, *Biomaterials* 2003, **24,**181.
14 J.-Z. Yang, R. Sultana, X.-Z. Hu and Z.-H. Huang, *J. Eur. Ceram. Soc.,* 2011, **31,** 2065.
15 J.-Z. Yang, R. Sultana, P. Ichim, X.-Z.Hu, Z.-H. Huang, W. Yi, B. Jiang, and Y.-G. Xu, *Ceram. Int.*, 2013, **39,** 6533.
16 J.-Z. Yang, R. Sultana and X.-Z. Hu, *Int. Appl. Ceram. Tech.,* 2014, **10,** 1.

17 S. Deville, E. Saiz, R. K. Nalla and A. P. Tomsia, *Science,* 2006, **311,** 515.
18 S. Deville, E. Saiz and A. P. Tomsia, *Biomaterials,* 2006, **27, 5480**.
19 P. Sepulveda, F. S. Ortega, M. D. M. Innocentini and V. C. Pandolfelli, *J. Am. Ceram. Soc.*, 2000, **83,** 3021.
20 J. Zeschky, T. Höfner, C. Arnold, R. Weißmann, D. Bahloul-Hourlier, M. Scheffler and P. Greil, *Acta Mater.,* 2005, **53,** 927.
21 B. Gates, Y.-D. Yin and Y.-N. Xia, *Chem. Mater.*, 1999, **11,** 2827.
22 A. Raksujarit, K. Pengpat, G. Rujijanagul and T. Tunkasiri, Mater. Des. 2010, **31,**1658.
23 J. M. Cordella, M. L. Vogl, and A. J. Wagoner Johnson, J. Mech. Behav. Biomed. Mater. 2009, **2,** 560.
24 B. H. Jones and T. P. Lodge, J. Am. Chem. Soc. 2009, **13,** 1676.
25 V. Bakumov, M. Schwarz, E. Kroke, J Eur. Ceram. Soc. 2009, **29,** 2857.
26 B. Viswanath and N. Ravishankar, *Scripta Mater.,* 2006, **55,** 863.
27 Huaxia Ji and P.M. Marquis, Biomaterials, 1992, **13,** 744.
28 R. Sultana, J.-Z. Yang, X.-Z. Hu, *J. Am. Ceram. Soc.,* 2012, **95,** 1212.
29 O. Gauthier, J.-M. Bouler, E. Aguado, P. Pilet and G. Daculsi, *Biomaterials* 1998, **19,** 133.
30 A. Bignon, J. Chouteau, J. Chevalier, G. Fantozzi, J.-P. Carret, P. Chavassieux, G. Boivin, M. Melin and D. Hartmann. *J. Mater. Sci. Mater. Med.,* 2003, **14,** 1089.
31 K. A. Hing, B. Annaz, S. Saeed, P. A. Revell and T. Buckland, *J. Mater. Sci. Mater. Med.*, 2005, **16,** 467.
32 M. Azami, F. Moztarzadeh and M. Tahriri, *J. Porous. Mater.,* 2010, **17,** 313.
33 J. R. Woodard, A. J. Hilldore, S. K. Lan, C. J. Park, A. W. Morgan, J. A. C. Eurell, S. G. Clark, M. B. Wheeler, R. D. Jamison and A. J. W. Johnson, *Biomaterials,* 2007, **28,** 45.
34 G.-B. Wei, P. X. Ma, Adv. Funct. Mater., 2008, **18,** 3568.
35 A. M. Lipski, C. Jaquiery, H. Choi, D. Eberli, M. Stevens, I. Martin, I. W. Chen, V. P. Shastri, Adv. Mater., 2007, **19,** 553.
36 J. D. Currey, *J. Exp. Biol.,* 1999, **202,** 2495.
37 Y. C. Fung, Springer-Verlag Inc., New York, 1993, p. 500.
38 Z.-J. Shen, E. Adolfsson, M. N., L.Gao, H. Kawaoka and K. Niihara, *Adv. Mater.,* 2001, **13,** 214.
39 S. Bose, S. Tarafder, S. S. Banerjee, N. M. Davies and A. Bandyopadhyay, *Bone,* 2011, **48,** 1282.
40 S. Bose and S. Tarafder, *Acta Biomater.,* 2012, **8,** 1401.
41 B. Palazzo, M. C. Sidoti, N. Roveri, A. Tampieri, M. Sandri, L. Bertolazzi, F. Galbusera, G. Dubini, P. Vena and R. Contro, *Mater. Sci. Eng. C* 2005, **25,** 207.
42 C. Wu and H. Zreiqat, *Acta Biomater.,* 2010, **6,** 820 .
43 E. A. Jackson and M. A. Hillmyer, *ACS Nano,* 2010, **4,** 3548.
44 B. G. Trewyn, S. Giri, I. I. Slowinga, V. S.-Y. Lin, *Chem. Commun.,* 2007, **31,** 3236.
45 Y. Lv, H. Liu, Z. Wang, S. Liu, L. Hao, Y. Sang, D. Liu, J. Wang, R. I. Boughton, *J. Membrane Sci.* 2009, **331,** 50.
46 M. Arkas , D. Tsiourvas and C. M. Paleos, *Chem. Mater.* 2005, **17,** 3439.
47 M. D. Sobsey, C. E. Stauber, L. M. Casanova, J. M. Brown and M. A. Elliott, *Environ. Sci. Technol.,* 2008**, 42**, 4261.
48 C. J. M. van Rijn, W. Nijdam, S. Kuiper, G. J Veldhuis, H. van Wolferen and M. Elwenspoek, *J. Micromech. Microeng.,* 1999, **9,** 170.
49 J. Cui, X. Zhang, H. Liu, S. Liu and K. L. Yeung, *J. Membrane Sci.* 2008, 325, 420.
50 R. Allabashi, M. Arkas, G. Hörmann and D. Tsiourvas, *Water Res.,* 2007, **41,** 476.
51 M. Ebrahimi, D. Willershausen, K. S. Ashaghi, L. Engel, L. Placido and P. Mund. *Desalination,* 2010, **250,** 991.
52 A. E. Pagana, S. D. Sklari, E. S. Kikkinides and V. T. Zaspalis, *Micropor. Mesopor. Mater.,* 2008, **110,** 150.
53 W.J. Koros and R. Mahajan, *J. Membrane Sci.* 2000, **175,** 181.
54 J.T. Richardson, Y. Peng and D. Remue, *Appl. Catalysis A: General,* 2000, **204**, 19.
55 B. R. Johnson, N. L. Canfield, D. N. Tran, R. A. Dagle, X. S. Li and J. D. Holladay, *Catalysis Today,* 2007, **120,** 54.
56 M. Zhou, T. Lin, F. Huang, Y. Zhong, Z.Wang and Y. Tang, *Adv. Funct. Mater.,* 2013, **23,** 2263.
57 A. Sommers, Q. Wang, X. Han, C. T'Joen, Y. Park and A. Jacobi, *Appl. Thermal Eng.,* 2010, **30,** 1277.
58 X.-D. Sun and J. A. Yeomans, *J. Mater. Sci.,* 1996, **31,** 875.
59 Z.-M. Xiu, Y. Liu, J.-G.Li, D. Huo, X.-D. Li, X.-D. Sun, K. Duan and X.-Z. Hu. Adv. Mater. Res., 2008, **41- 42,** 41.